Int. J. Solids Structures Vol. 27, No. 5, pp. 585–599, 1991
Printed in Great Britain.

0020-7683/91 $3.00 + .00

BENDING, VIBRATION AND STABILITY OF ARALL® LAMINATES USING A GENERALIZED LAMINATE PLATE THEORY

J. L. TEPLY
Alcoa Laboratories, Alcoa Center, PA 15069, U.S.A.

E. J. BARBERO
Department of Mechanical and Aerospace Engineering, West Virginia University, Morgantown, WV 26506-6101, U.S.A.

and

J. N. REDDY
Department of Engineering Science and Mechanics, Virginia Polytechnic Institute and State University, Blacksburg, VA 24061, U.S.A.

(*Received* 7 *September* 1989; *in revised form* 1 *March* 1990)

Abstract—A plate bending element based on the generalized laminate plate theory (GLPT) is used to evaluate new composite laminates known as the ARALL-1® Laminates. The plate finite element accounts for the transverse shear deformation and layer-wise description of the displacements. The finite element is used to evaluate the stresses, vibration and buckling characteristics of 2/1 and 3/2 ARALL Laminates.

1. BACKGROUND

Laminated composite plates are often modelled using the classical laminate plate theory (CLPT) or the first-order shear deformation plate theory (FSDT). In both cases the laminate is treated as a single-layer plate with equivalent stiffnesses, and the displacements are assumed to vary through the thickness according to a single expression (see Reddy, 1984, 1989a,b), not allowing for possible discontinuities in strains at an interface of dissimilar material layers. A laminate made of flexible layers next to stiff layers will experience such discontinuous strains.

Recently, Reddy (1987) presented a laminate plate theory that allows piece-wise representation of displacements through individual lamina of a laminate. In the generalized laminate plate theory (GLPT), the equations of three-dimensional elasticity are reduced to differential equations in terms of unknown functions in two dimensions, by assuming layer-wise approximation of the displacements through the thickness. Exact analytical solutions of the theory were developed by Barbero (1989) and Barbero *et al.* (1990) to evaluate the accuracy of the theory compared to the 3-D elasticity theory. The results indicated that the generalized laminate plate theory allows accurate determination of interlaminar stresses.

The present paper deals with the application of Reddy's generalized plate theory to ARALL Laminates. ARALL Laminates are hybrid laminates in which layers of aramid-epoxy are placed between thin, high-strength aluminium alloy layers (see Bucci *et al.*, 1988). They are produced as sheet materials in a normal autoclave bonding cycle. ARALL Laminates were primarily developed as materials with good damage tolerance properties. They combine low density and high strength properties, and therefore are very attractive for aerospace applications. The designations 2/1 and 3/2 correspond to (Al/Ar/Al) and (Al/Ar/Al/Ar/Al), respectively (see Fig. 1). Each aramid layer is modelled as three layers. The middle layer represents the fiber-rich part of the aramid layer, and the layers on either side represent resin-rich parts that bond the aramid fiber to the aluminium layers. In this study, aluminium layers are taken to be 0.03048 mm thick, fiber-rich layers 0.0144 mm thick and resin-rich layers 0.0072 mm thick. Thus, ARALL 2/1 is modelled as a six-layer laminate (Al/resin/Ar)$_s$. ARALL 3/2 is modelled using 10 layers (Al/resin/Ar/resin/Al)$_s$.

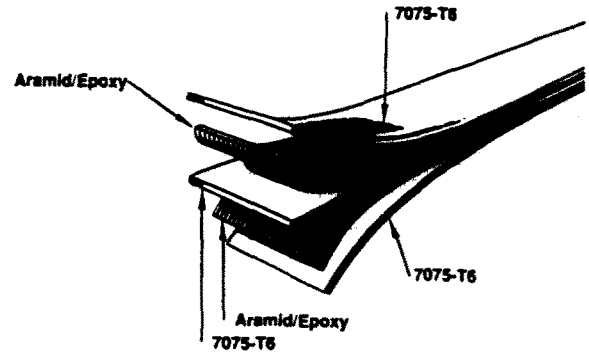

Schematic of ARALL-1

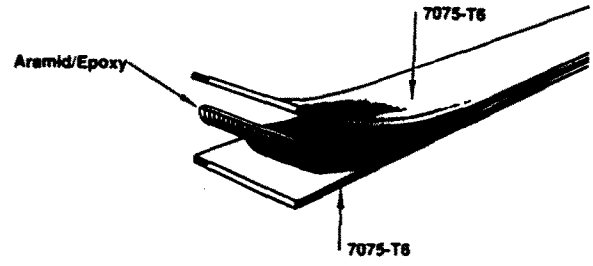

Schematic of Test Panels

Fig. 1. The ARALL 2/1 and 3/2 Laminates.

In the interest of brevity, only the main equations of the theory are reviewed and the major steps of the formulation are presented. The analysis is performed using the plate bending element developed by Reddy *et al.* (1989). Application of the element to ARALL Laminates is the main focus of this study.

2. A REVIEW OF GLPT

Consider a laminated plate composed of N orthotropic lamina, each being oriented arbitrarily with respect to the laminate (x, y) coordinates, which are taken to be in the midplane of the laminate. The displacements (u_1, u_2, u_3) at a point (x, y, z) in the laminate are assumed to be of the form

$$\begin{aligned} u_1(x, y, z) &= u(x, y) + U(x, y, z) \\ u_2(x, y, z) &= v(x, y) + V(x, y, z) \\ u_3(x, y, z) &= w(x, y), \end{aligned} \tag{1}$$

where (u, v, w) are the displacement of a point $(x, y, 0)$ on the reference plane of the laminate, and U and V are functions which vanish on the reference plane:

$$U(x, y, 0) = V(x, y, 0) = 0. \tag{2}$$

In order to reduce the three-dimensional theory to a two-dimensional one, we assume that U and V are approximated as

$$\begin{aligned} U(x, y, z) &= \sum_{j=1}^{n} U_j(x, y)\phi^j(z) \\ V(x, y, z) &= \sum_{j=1}^{n} V_j(x, y)\phi^j(z), \end{aligned} \tag{3}$$

where U_j and V_j are undetermined coefficients, and ϕ^j are any continuous functions that

satisfy the condition

$$\phi^j(0) = 0 \quad \text{for all } j = 1, 2, \ldots, n. \tag{4}$$

Note that the transverse deflection here is assumed to be independent of the thickness coordinate, an assumption often used in most plate theories. This amounts to the neglect of the transverse normal stress.

The approximation in eqn (3) can also be viewed as the global semi-discrete finite-element approximations of U and V through thickness. In that case ϕ^j denote the global interpolation functions, and U_j and V_j are the global nodal values of U and V (and possibly their derivatives) at the nodes through the thickness of the laminate. For example, a finite-element approximation based on the Lagrangian interpolation through thickness can be obtained from eqn (3) by setting [if the midplane does not coincide with an interface, it is used as an interface to satisfy eqn (2)], $n = pN + 1$, where

N = number of layers through thickness;
P = degree of the global interpolation polynomials, $\phi^j(z)$; and
U_j, V_j = global nodal values of U and V.

For example, if a piece-wise linear displacement distribution is chosen, the corresponding functions $\phi^j(z)$ are

$$\phi^j(z) = \begin{cases} \dfrac{z - z_{j-1}}{z_j - z_{j-1}}; & z_{j-1} < z < z_j \\ \dfrac{z_{j+1} - z}{z_{j+1} - z_j}; & z_j < z < z_{j+1} \end{cases}$$

where z_j denote the global thickness coordinate of the node between the jth and the $(j+1)$th layers.

The equilibrium equations of the theory can be derived using the principle of virtual displacements (see Reddy, 1984),

$$\begin{aligned} 0 = \int_\Omega \Bigg\{ & N_x \left(\frac{\partial \delta u}{\partial x}\right) + N_y \left(\frac{\partial \delta v}{\partial y}\right) + N_{xy} \left(\frac{\partial \delta u}{\partial y} + \frac{\partial \delta v}{\partial x}\right) \\ & + Q_x \frac{\partial \delta w}{\partial x} + Q_y \frac{\partial \delta w}{\partial y} + \sum_{j=1}^{n} \Bigg[N_x^j \frac{\partial \delta U_j}{\partial x} + N_y^j \frac{\partial \delta V_j}{\partial y} \\ & + N_{xy}^j \left(\frac{\partial \delta U_j}{\partial y} + \frac{\partial \delta V_j}{\partial x}\right) + Q_x^j U_j + Q_y^j V_j \Bigg] - q \delta w \Bigg\} \mathrm{d}A, \end{aligned} \tag{5a}$$

where

$$\begin{aligned} (N_x, N_y, N_{xy}) &= \int_{-h/2}^{h/2} (\sigma_x, \sigma_y, \sigma_{xy})\, \mathrm{d}z \\ (Q_x, Q_y) &= \int_{-h/2}^{h/2} (\sigma_{xz}, \sigma_{yz})\, \mathrm{d}z \\ (N_x^j, N_y^j, N_{xy}^j) &= \int_{-h/2}^{h/2} (\sigma_x, \sigma_y, \sigma_{xy}) \phi^j(z)\, \mathrm{d}z \\ (Q_x^j, Q_y^j) &= \int_{-h/2}^{h/2} (\sigma_{xz}, \sigma_{yz}) \frac{\mathrm{d}\phi^j(z)}{\mathrm{d}z} \mathrm{d}z, \end{aligned} \tag{5b}$$

$(\sigma_x, \sigma_y, \sigma_{xy}, \sigma_{xz}, \sigma_{yz})$ are the stresses and q is the distributed transverse load. The virtual work statement in eqn (5a) gives $(2n+3)$ differential equations in $(2n+3)$ variables (u, v, w, U_j, V_j). The form of the geometric and force boundary conditions is given below:

Geometric (Essential)	Force (Natural)
u	$N_x n_x + N_{xy} n_y$
v	$N_{xy} n_x + N_y n_y$
w	$Q_x n_x + Q_y n_y$
U_j	$N_x^j n_x + N_{xy}^j n_y$
V_j	$N_{xy}^j n_x + N_y^j n_y$

(6)

where (n_x, n_y) denote the direction cosines of a unit normal to the boundary of the midplane Ω.

The constitutive equations of the laminate are given by

$$\{N\} = [A]\{e\} + \sum_{k=1}^{n} [B^k]\{e_k\} \tag{7a}$$

$$\{N^j\} = [B^j]\{e\} + \sum_{k=1}^{n} [D^{jk}]\{e_k\}, \tag{7b}$$

where the strains $\{e\}$ and $\{e_k\}$, and the matrices $[A]$, $[B^j]$ and $[D^{jk}]$ are given in Reddy (1987); also see the Appendix.

3. FINITE-ELEMENT FORMULATION

The displacements (u, v, w, U_j, V_j) are expressed, over each element, as a linear combination of the 2-D shape functions (ψ_i) and the nodal values $(u_i, v_i, w_i, U_j^i, V_j^i)$ as follows:

$$(u, v, w, U_j, V_j) = \sum_{i=1}^{m} (u_i, v_i, w_i, U_j^i, V_j^i)\psi_i \tag{8}$$

where m is the number of nodes per element.

Using eqn (8), the strains can be expressed in the form

$$\{e\} = [H]\{u\}, \{e^j\} = [H^j]\{U^j\} \tag{8a}$$

where

$$\{u\} = \begin{Bmatrix} u \\ v \\ w \end{Bmatrix}, \quad \{U^j\} = \begin{Bmatrix} U_j^i \\ V_j^i \end{Bmatrix}. \tag{8b}$$

The matrices $[H]$ and $[H^j]$ are given in the Appendix.

Using eqns (8) in the virtual work statement, we obtain the finite element model (see Reddy *et al.*, 1989)

$$[K]\{U\} = \{F\}. \tag{9}$$

4. INTERLAMINAR STRESS CALCULATION

When a piece-wise linear interpolation through the thickness is used, GLPT provides an excellent representation of the displacements, and an accurate prediction of the in-

plane stresses ($\sigma_{xx}, \sigma_{yy}, \sigma_{xy}$) as demonstrated by Barbero *et al.* (1990). Interlaminar stresses ($\sigma_{xz}, \sigma_{yz}, \sigma_{zz}$) are easily computed from the equilibrium equations of 3-D-elasticity when exact analytical solutions are available. An approximate technique is used in this study to integrate the equilibrium equations, using the in-plane stress information provided by the finite element solution. The scheme as presented by Chaudhuri (1987), is extended here to quadrilateral isoparametric elements. It approximates the shear stress distribution through each layer with a quadratic function, thus requiring $3N$ equations for each of the shear stresses (σ_{xz}, σ_{yz}), where N is the number of layers. Here, N equations are used to satisfy the (N) average shear stresses on each layer. Two equations are used to impose vanishing shear stresses at the surfaces of the plate. Then, $(N-1)$ equations are employed to satisfy continuity of the shear stresses at the interfaces between layers. Finally, the remaining $(N-1)$ equations are used to compute the jump in $\sigma_{xz,z}$ (or $\sigma_{yz,z}$) at each interface.

The average shear stresses on each layer are computed from the constitutive equations and the displacement field obtained in the finite-element analysis.

In this work, the following equilibrium equations

$$\sigma_{xz,z} = -(\sigma_{xx,x} + \sigma_{xy,y}) \qquad \sigma_{yz,z} = -(\sigma_{xy,x} + \sigma_{yy,y}) \tag{10}$$

are used to compute $\sigma_{xz,z}$ and $\sigma_{yz,z}$ directly from the finite-element approximation. The in-plane components of the stresses and their in-plane derivatives ($\sigma_{xx,x}$; $\sigma_{yy,y}$; $\sigma_{xy,x}$ and $\sigma_{xy,y}$) are computed from the constitutive equations for each layer, i.e.

$$\begin{Bmatrix} \sigma_x \\ \sigma_y \\ \sigma_{xy} \end{Bmatrix} = \begin{bmatrix} Q_{11} Q_{12} Q_{13} \\ Q_{12} Q_{22} Q_{23} \\ Q_{13} Q_{23} Q_{33} \end{bmatrix} \begin{Bmatrix} \dfrac{\partial u}{\partial x} + \displaystyle\sum_{j=1}^{n} \frac{\partial U_j}{\partial x} \phi^j \\ \dfrac{\partial v}{\partial x} + \displaystyle\sum_{j=1}^{n} \frac{\partial V_j}{\partial x} \phi^j \\ \dfrac{\partial u}{\partial y} + \dfrac{\partial v}{\partial x} + \displaystyle\sum_{j=1}^{n} \left(\frac{\partial V_j}{\partial y} + \frac{\partial V_j}{\partial x} \right) \phi^j \end{Bmatrix}. \tag{11}$$

The procedure thus requires computation of second derivatives of the displacements (u, v, U_j, V_j), which can be obtained from the finite element approximation (see Reddy, 1986, Problem 7-2-11, p. 435).

5. DISCUSSION OF THE RESULTS

Bending analysis

The bending behavior of ARALL Laminates under uniform transverse loading is studied. A simply-supported square laminate is considered. In order to assess the effect of the thickness ratio on the response, the following non-dimensionalizations are used:

$$(\bar{\sigma}_x, \bar{\sigma}_y, \bar{\sigma}_{xy}) = (\sigma_x, \sigma_y, \sigma_{xy}) \frac{1}{qs^2}$$

$$(\bar{\sigma}_{yz}, \bar{\sigma}_{xz}) = (\sigma_{yz}, \sigma_{xz}) \frac{1}{qs}$$

$$\bar{w} = \frac{100 E_{Al}}{qhs^4} w, \quad (\bar{u}, \bar{v}) = \frac{100 E_{Al}}{qhs^3} (u, v) \tag{12}$$

where q is the intensity of the uniform transverse load. ARALL 2/1 is modelled as a six-layer laminate (Al/resin/aramid)$_s$. ARALL 3/2 is modelled using 10 layers representing the different materials in the same form as for ARALL 2/1.

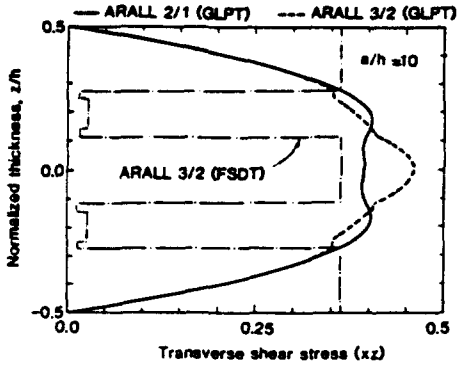

Fig. 2. Through-the-thickness distribution of the transverse shear stress σ_{xz} in simply-supported ARALL 2/1 and ARALL 3/2 plates under uniform load.

The material properties used are,

aluminium:

$$E = 10.4 \times 10^6 \text{ psi}, \quad \nu = 0.333;$$

resin-rich aramid:

$$E_1 = 2.196 \times 10^6 \text{ psi}, \quad E_2 = 4.8219 \times 10^5 \text{ psi}$$
$$G_{12} = 1.5717 \times 10^5 \text{ psi}, \quad G_{23} = 1.5576 \times 10^5 \text{ psi}$$
$$\nu_{12} = 0.3749, \quad \nu_{23} = 0.5479;$$

fiber-rich aramid:

$$E_1 = 1.2549 \times 10^7 \text{ psi}, \quad E_2 = 7.6525 \times 10^5 \text{ psi}$$
$$G_{12} = 2.8955 \times 10^5 \text{ psi}, \quad G_{23} = 2.6462 \times 10^5 \text{ psi}$$
$$\nu_{12} = 0.3458, \quad \nu_{23} = 0.4459. \tag{13}$$

Due to symmetry, only a quarter (upper right quadrant) of the plate is modelled using a 4×4 mesh of eight-node isoparametric elements.

Both in-plane and interlaminar shear stresses can be computed using either the constitutive equations or equilibrium equations. In-plane stresses are linear in each layer and they approximate closely the exact solution. Interlaminar shear stresses are constant in each layer, their value being approximately the average of the exact solution. It is also possible to obtain the actual distribution of interlaminar shear stresses by a post-processing algorithm (see Section 4) if the solution is obtained using quadratic elements.

For all cases the stresses are presented as a function of the non-dimensional thickness z/h. The results shown correspond to values at the Gauss points closest to the points where the solution has a maximum, i.e. $\sigma_{xx}(\alpha, \alpha, z)$, $\sigma_{yy}(\alpha, \alpha, z)$, $\sigma_{xy}(\beta, \beta, z)$, $\sigma_{xz}(\beta, \alpha, z)$, $\sigma_{yz}(\alpha, \beta, z)$, with $\alpha = 0.526\,a$ and $\beta = 0.973a$. The simply-supported boundary conditions used are :

$$w(0, y) = w(a, t) = v(0, y) = v(a, y) = V_j(0, y) = V_j(a, y) = 0,$$
$$w(x, 0) = w(x, b) = u(x, 0) = u(x, b) = U_j(x, 0) = U_j(x, b) = 0. \tag{14}$$

The symmetry along the centerline implies that,

$$u(a/2, y) = U^j(a/2, y) = 0,$$
$$v(x, b/2) = V^j(s, b/2) = 0 \tag{15}$$

where $j = 1, \ldots, N$, and N is the number of layers in the laminate.

From the distribution of interlaminar, transverse shear stresses (Figs 2 and 3), we can observe that the maximum occurs in the aluminium layers, either at the outer layers for

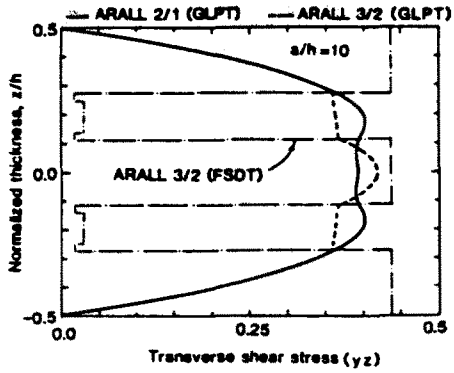

Fig. 3. Through-the-thickness distribution of the transverse shear stress σ_{yz} in simply-supported ARALL 2/1 and ARALL 3/2 plates under uniform load.

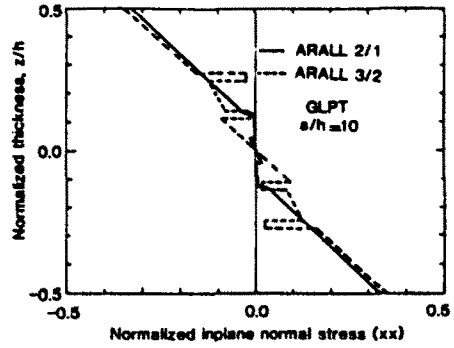

Fig. 4. Through-the-thickness distribution of the in-plane normal stress σ_{xx} in simply-supported ARALL 2/1 and ARALL 3/2 plates under uniform load.

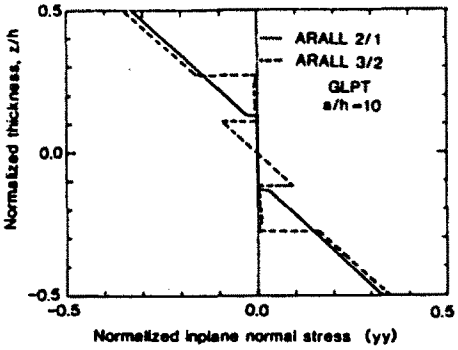

Fig. 5. Through-the-thickness distribution of the in-plane normal stress σ_{yy} in simply-supported ARALL 2/1 and ARALL 3/2 plates under uniform load.

ARALL 2/1 or at the center layer for ARALL 3/2. This may be an advantageous factor because the matrix material has low strength in shear. The first-order shear deformation theory (FSDT) predicts even lower shear stresses at the aramid layers. For hybrid composites like ARALL Laminates, the shear strain distribution is not a constant, contrary to the assumption made in FSDT. Therefore, large shear strains do occur in the more compliant aramid layers thus relaxing the shear stresses through the laminate. However, shear stresses do not reach high values in the compliant layers due to the low shear moduli of the aramid. As a result, an optimization with respect to shear failure can be accomplished by the use of compliant layers.

Plots of the in-plane stresses, σ_{xx} and σ_{yy} along the fiber direction and perpendicular to the fibers, are shown in Figs 4 and 5, where it can be observed that the resin-rich layers

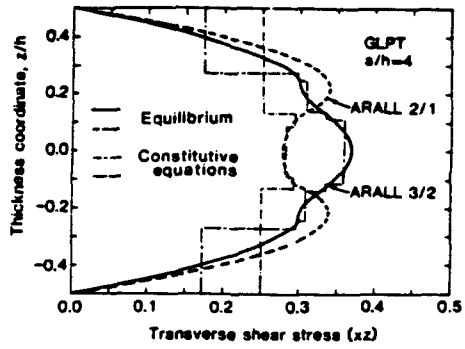

Fig. 6. Comparison between σ_{xz} obtained from constitutive equations and equilibrium equations using quadratic elements.

are subject to very low stresses and that the in-plane stress is carried by the aluminium layers for both kind of laminates. The in-plane stresses reported here do not include the residual stresses due to pre-straining of ARALL-1 Laminates. The mechanics of the pre-straining of ARALL-1 Laminates are described by Teply *et al.* (1987). Thus, the actual stresses will be the sum of the residual stresses and stresses shown in Figs 4–5.

The transverse shear stress σ_{xz} computed from equilibrium equations (continuous curves) and those computed from constitutive equations (discontinuous lines) are shown in Fig. 6. Quadratic elements are used to obtain both stress fields. Of course, to obtain the transverse shear stresses from the constitutive equations one can even use linear finite elements. Figure 7 contains a comparison of σ_{xz} computed from the constitutive equations using linear finite elements, with that obtained using equilibrium equations and quadratic elements. It is observed that the discontinuous stress fields, computed from the constitutive equations, agree closely with the average of those computed from equilibrium.

The maximum transverse deflections versus side-to-thickness ratio are shown in Fig. 8. It is clear that the deflections obtained by the FSDT are lower than those predicted by the GLPT. We can also see from Fig. 9 that there is appreciable difference in the maximum in-plane stresses obtained using the FSDT and GLPT, when the aspect ratio is $a/h = 4$. In general, in the GLPT models, the composite laminates are relatively more flexible than by FSDT. The GLPT allows relative flexibility between stiff and less stiff layers.

A comparison of the response of ARALL Laminates and aluminium is presented in Figs 10–14. The distribution of in-plane stresses σ_{xx}, σ_{yy} and σ_{xy} is shown in Figs 10–12. It is evident that the stress distributions in the aluminium layers are not much affected by the presence of the aramid layers. The aramid layers are subjected to low stress levels, which guarantees an extended life for the aramid material. Note that the residual stresses should be added to the σ_{xx} and σ_{yy} stresses (see Teply *et al.*, 1987). The interlaminar shear stresses

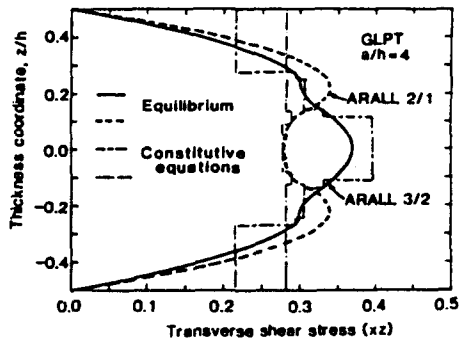

Fig. 7. Comparison between σ_{xz} obtained from constitutive equations (using linear elements) and equilibrium equations (using quadratic elements).

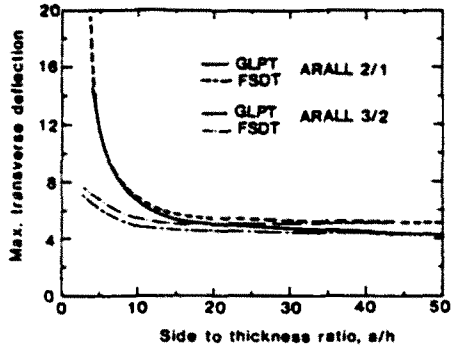

Fig. 8. Transverse deflections vs side-to-thickness ratio of simply-supported ARALL Laminates under uniform load.

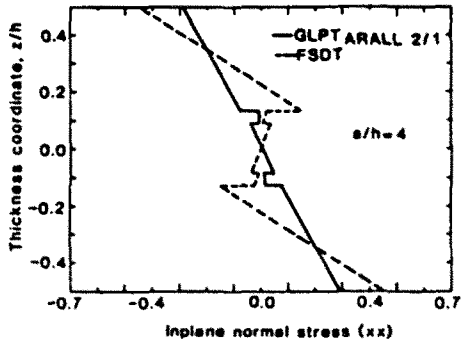

Fig. 9. Comparison of the through-the-thickness distribution of the in-plane normal stress σ_{xx} in a simply-supported ARALL 2/1 plate under uniform load.

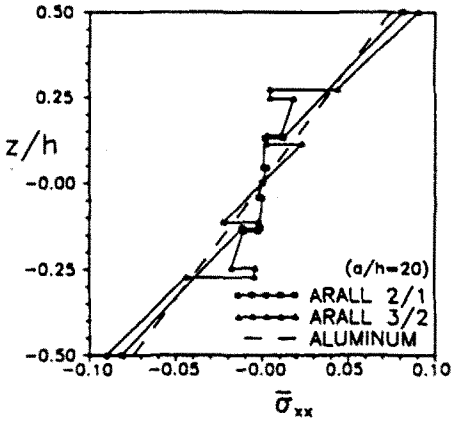

Fig. 10. Comparison of the through-the-thickness distribution of the in-plane normal stress σ_{xx} in simply-supported ARALL Laminates and aluminium plates.

σ_{xz} and σ_{yz} are reduced by the presence of the more compliant aramid layers, as shown in Figs 13 and 14 for both the 2/1 and 3/2 lamination sequences.

Vibration results

The vibration of ARALL Laminates and aluminium plates was investigated using GLPT and CPT. The effects of rotary and in-plane inertia on the vibration of simply-supported rectangular plates were investigated. Numerical results are presented for various values of the aspect ratio a/b and thickness ratio a/h. It can be seen from Table 1 that CPT

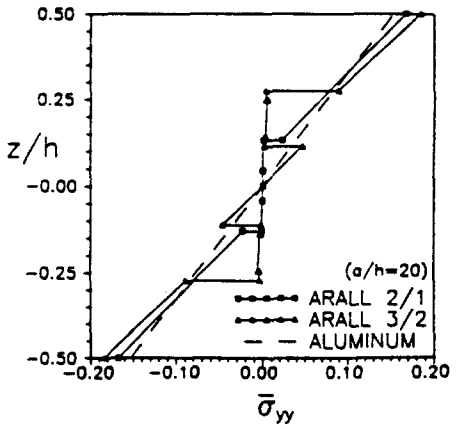

Fig. 11. Comparison of the through-the-thickness distribution of the in-plane normal stress σ_{yy} in simply-supported ARALL Laminates and aluminium plates.

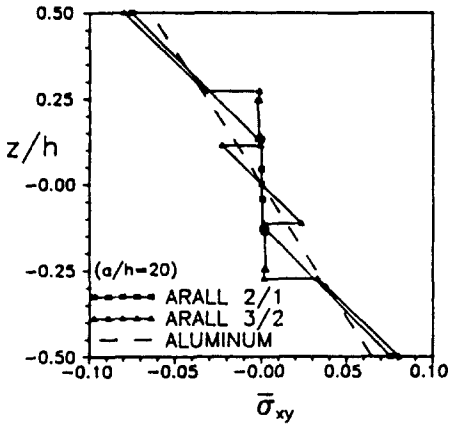

Fig. 12. Comparison of the through-the-thickness in-plane shear stress σ_{xy} in simply-supported ARALL Laminates and aluminium plates.

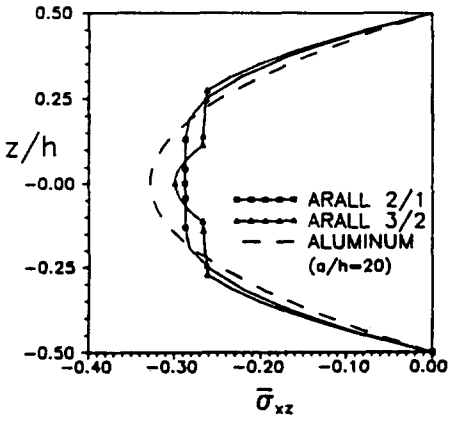

Fig. 13. Comparison of the through-the-thickness transverse shear stress σ_{xz} in simply-supported ARALL Laminates and aluminium plates.

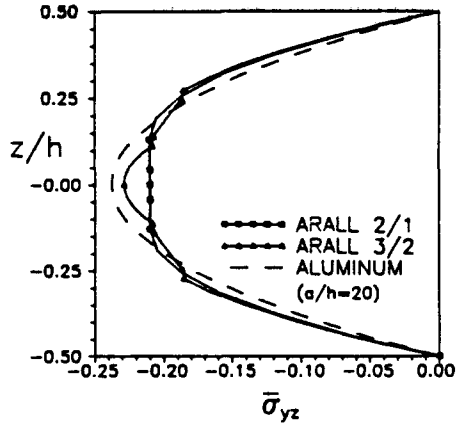

Fig. 14. Comparison of the through-the-thickness transverse shear stress σ_{yz} in simply-supported ARALL Laminates and aluminium plates.

gives closer results for isotropic materials, while larger differences between CPT and GLPT can be observed for ARALL Laminates. This is because the hybrid nature of ARALL Laminates is correctly represented in GLPT, while the different materials are smeared out in CPT.

Since ARALL Laminates are symmetric, the inclusion of in-plane inertia does not affect the transverse natural frequency. This is because in-plane and transverse deflections are uncoupled for symmetric laminates. The results shown in Tables 1, 2 and 3 can be explained as follows. The frequency ω is related to the stiffness K and mass M by the

Table 1. Fundamental frequency $\bar{\omega} = \omega \frac{ab}{h}\sqrt{\frac{\rho_{Al}}{E_{Al}}}$ for $a/b = 1$.

a/h	Theory	Rotary inertia	Inplane inertia	Al	ARALL 2/1	ARALL 3/2
10	GLPT	yes	yes	5.84530	5.06894	5.10272
		no	yes	5.88853	5.08869	5.12564
		yes	no	5.84530	5.06894	5.10272
		no	no	5.88530	5.08869	5.12564
	CPT	no	no	6.04287	6.32473	6.07226
5	GLPT	yes	yes	5.36859	3.70444	3.78094
		no	yes	5.48859	3.72641	3.80310
		yes	no	5.36859	3.70444	3.78094
		no	no	5.48859	3.72641	3.80310
	CPT	no	no	6.04287	6.32473	6.07226
20	GLPT	yes	yes	5.99115	5.90821	5.77432
		no	yes	6.00313	5.91849	5.78481
		yes	no	5.99115	5.90821	5.77432
		no	no	6.00313	5.91849	5.78481
	CPT	no	no	6.04287	6.32473	6.07226
50	GLPT	yes	yes	6.03448	6.25107	6.02150
		no	yes	6.03646	6.25324	6.02356
		yes	no	6.03448	6.25107	6.02150
		no	no	6.03646	6.25324	6.02356
	CPT	no	no	6.04287	6.32473	6.07226
100	GLPT	yes	yes	6.04077	6.30603	6.05974
		no	yes	6.04126	6.30660	6.06027
		yes	no	6.04077	6.30603	6.05974
		no	no	6.04126	6.30660	6.06027
	CPT	no	no	6.04287	6.32473	6.07226

Table 2. Fundamental frequency $\bar{\omega} = \omega \frac{ab}{h}\sqrt{\frac{\rho_{Al}}{E_{Al}}}$ for $a/b = 2$.

a/h	Theory	Rotary inertia	Al	ARALL 2/1	ARALL 3/2
5	GLPT	yes	5.89692	3.58746	3.49686
	GLPT	no	6.10834	3.62144	3.51801
	CPT	no	7.55369	7.90325	7.49241
10	GLPT	yes	6.98593	5.22132	5.30423
	GLPT	no	7.09747	5.24796	5.33507
	CPT	no	7.55369	7.90325	7.49241
20	GLPT	yes	7.39581	6.78216	6.67933
	GLPT	no	7.43135	6.80344	6.70291
	CPT	no	7.55369	7.90325	7.49241
50	GLPT	yes	7.52759	7.67882	7.34018
	GLPT	no	7.53371	7.68505	7.34617
	CPT	no	7.55369	7.90325	7.49241
100	GLPT	yes	7.54714	7.34499	7.45338
	GLPT	no	7.54869	7.84672	7.45499
	CPT	no	7.55369	7.90325	7.49241

relation,

$$\omega \sim \sqrt{\frac{K}{M}}.$$

The fundamental frequency of an ARALL Laminate depends on the transverse stiffness (i.e. stiffness coefficients D_{22}), which is smaller than the axial stiffness (i.e. stiffness coefficient D_{11}). Because of the specific construction of ARALL Laminates, it can be established that the following stiffness and mass inequalities hold:

$$K_{Al} > K_{21} > K_{12}; \quad M_{Al} > M_{21} > M_{32}$$

where subscripts "Al", "21" and "32" refer to aluminium, 2/1 Laminates and 3/2 Laminates, respectively. The above inequalities imply the following two cases of inequalities between 2/1 and 3/2 ARALL Laminates:

$$\text{Case one}: K_{21}M_{32} > K_{32}M_{21}$$

$$\text{Case two}: K_{21}M_{32} < K_{32}M_{21}.$$

Table 3. Fundamental frequency $\bar{\omega} = \omega \frac{ab}{h}\sqrt{\frac{\rho_{Al}}{E_{Al}}}$ for $a/b = 5$.

a/h	Theory	Rotary inertia	Al	ARALL 2/1	ARALL 3/2
5	GLPT	yes	7.8585	4.9407	4.1486
	GLPT	no	7.8525	2.8837	4.2060
	CPT	no	15.7120	16.4380	15.5454
10	GLPT	yes	11.6442	6.9430	6.6198
	GLPT	no	15.0222	7.0256	6.6620
	CPT	no	15.7120	16.4380	15.5454
20	GLPT	yes	14.2346	10.1474	10.2947
	GLPT	no	14.5105	10.2031	10.3555
	CPT	no	15.7120	16.4380	15.5353
50	GLPT	yes	15.4370	14.4124	14.0980
	GLPT	no	15.4994	14.4533	14.1423
	CPT	no	15.7120	16.4380	15.5454
100	GLPT	yes	15.6415	15.8379	15.1381
	GLPT	no	15.6580	15.8541	15.1538
	CPT	no	15.71201	16.4380	15.5454

Table 4. Buckling load $\bar{N} = \frac{Na^2}{E_{Al}h^3}$ perpendicular to the fiber direction of ARALL 2/1 and 3/2 compared to aluminium plates

	Al		ARALL 2/1		ARALL 3/2	
a/h	CPT	GLPT	CPT	GLPT	CPT	GLPT
10	3.7	2.1924	3.6396	0.1478	3.2685	1.1380
20	3.7	3.1350	3.6396	0.5923	3.2685	2.1119
30	3.7	3.4171	3.6396	1.1998	3.2685	2.5206
40	3.7	3.5334	3.6396	1.7834	3.2685	2.7321
50	3.7	3.5914	3.6396	2.2489	3.2685	2.8622
100	3.7	3.6740	3.6396	3.2201	3.2685	3.1241
1000	3.7	3.7027	3.6396	3.6385	3.2685	3.2692

Similar inequalities hold for aluminium and 2/1 or 3/2 ARALL Laminates. If Case one holds then $\omega_{21} > \omega_{32}$ (i.e. the fundamental frequency of 2/1 Laminates is greater than that of 3/2 Laminates), and if Case two holds then $\omega_{21} < \omega_{32}$. Similarly, if we replace K_{32} and M_{32} by K_{al} and M_{al}, we arrive at the inequalities:

$$\omega_{21} > \omega_{al}, \text{ when Case one holds}$$

and

$$\omega_{21} < \omega_{al}, \text{ when Case two holds.}$$

In the present study Case one is valid for thin laminates (i.e. $a/h \geqslant 20$) and Case two is valid for thick laminates (i.e. $a/h < 20$). For thick laminates, while the mass remains the same as for thin laminates, the stiffness is reduced due to transverse shear deformation. Of course Case two holds in the classical plate theory for all side-to-thickness ratios. Tables 2 and 3 show that the differences between the results of GLPT and CPT are more evident as the aspect ratios a/b increase. From the results, it is evident that ARALL Laminates exhibit lower fundamental frequencies than aluminium plates for moderate to large thickness ratios (i.e. $a/h < 20$). This is because the reduced flexural rigidity, due to the presence of layers with low shear moduli, outweighs the effect of the slightly lower density of ARALL Laminates. For large thickness ratios (i.e. $a/h > 20$), both effects cancel out, and the aluminium plates, 3/2 and 2/1 Laminates exhibit increasingly large frequencies.

Buckling results

Buckling loads N_x and N_y are presented in Tables 4 and 5 for simply supported aluminium, ARALL 2/1 and 3/2 Laminates. The in-plane load is uniformly distributed along $x = a/2$ for Table 4, and along $y = b/2$ for Table 5. The minimum buckling load corresponds, at $a/b = 1$, to mode $m = 1$ for all thickness ratios from 10 to 1000. The results given by GLPT are compared with CPT. It is noted that the CPT non-dimensional values are independent of a/h. The buckling loads predicted by GLPT are smaller for low a/h due to shear deformation as expected. While there is a good correlation between CPT and GLPT for aluminium plates, the CPT values deteriorate for low a/h on the ARALL

Table 5. Buckling load $\bar{N} = \frac{Nb^2}{E_{Al}h^3}$ in the fiber direction of ARALL 2/1 and 3/2 compared to aluminium plates

	Al		ARALL 2/1		ARALL 3/2	
a/h	CPT	GLPT	CPT	GLPT	CPT	GLPT
10	3.7	2.1924	3.6396	0.4443	3.2685	0.9062
20	3.7	3.1350	3.6396	1.1950	3.2685	1.8651
30	3.7	3.4171	3.6396	1.8023	3.2685	2.3365
40	3.7	3.5334	3.6396	2.2473	3.2685	2.5944
50	3.7	3.5914	3.6396	2.5716	3.2685	2.7553
100	3.7	3.6740	3.6396	3.2779	3.2685	3.0826
1000	3.7	3.7027	3.6396	3.6386	3.2685	3.2682

Laminates. This is because the deformations through the thicknesses of hybrid materials depart from the assumptions used in CPT.

By comparing the results of the two tables we observe that the CPT value does not change with the direction of the load. The critical buckling load predicted by CPT for simply-supported, generally orthotropic square plates, under a uniform in-plane load is

$$N = \left(\frac{\pi}{b}\right)^2 [D_{11} + D_{22} + 2(D_{12} + 2D_{66})].$$

When the direction of the load changes from 0° to 90°, the coefficients D_{11} and D_{22} exchange their values and the above expression gives the same buckling load. Furthermore, typical values of these coefficients for ARALL 2/1 Laminates are:

$$D_{11} = 961261 \text{ psi}$$
$$D_{22} = 958063 \text{ psi}.$$

Therefore, even if the load is changed from the fiber direction to an angle different from 90°, the buckling load will remain almost constant. The GLPT does not predict identical values due to the consideration of shear deformation, but the results follow the same trend.

6. CONCLUSIONS

The generalized laminate plate theory of Reddy (1987) is used to evaluate the static and dynamic response of ARALL Laminates. The generalized laminate theory yields accurate results for displacements, stresses, natural frequencies and buckling loads. While the GLPT plate bending element is computationally expensive compared to the FSDT plate element (or the Minlin plate element), it yields accurate results for all stresses and is less expensive compared to a three-dimensional finite element analysis of laminated composite plates.

REFERENCES

Barbero, E. J. (1989). On a generalized laminate theory with application to bending, vibration, and delamination buckling in composite laminates. Ph.D. Dissertation, Virginia Polytechnic Institute and State University, Blacksburg, VA 24061, U.S.A.

Barbero, E. J., Reddy, J. N. and Teply, J. L. (1990). An accurate determination of stresses in thick laminates using a generalized plate theory. *Int. J. Num. Meth. Engng* **29**, 1–14.

Bucci, R. J. *et al.* (1988). ARALL laminates properties and design update. 33*rd Int. SAMPE Symp.*, Anaheim, CA.

Chaudhuri, R. A. (1987). An approximate semi-analytical method for prediction of interlaminar shear stress in an arbitrarily laminated thick plate. *Comput. Struct.* **25**(4), 627–636.

Reddy, J. N. (1984). *Energy and Variational Methods in Applied Mechanics*. John Wiley, NY.

Reddy, J. N. (1986). *Applied Functional Analysis and Variational Methods in Engineering*. McGraw-Hill, NY.

Reddy, J. N. (1987). A generalization of two-dimensional theories of laminated composite plates. *Commun. Appl. Numer. Meth.* **3**, 173–180.

Reddy, J. N. (1989a). On the generalization of displacement-based laminate plate theories. *Appl. Mech. Rev.* **42**(11), Part 2, S213–S222.

Reddy, J. N. (1989b). On refined computational models of composite laminates. *Int. J. Num. Meth. Engng* **27**, 361–382.

Reddy, J. N., Barbero, E. J. and Teply, J. L. (1989). A plate bending element based on a generalized laminate theory. *Int. J. Num. Meth. Engng* **28**, 2275–2392.

Teply, J. L. Redd, S. M., and Schultz, R. W. (1987). Performance mechanics of ARALL laminates. *First International SAMPE Metals Conf.* 18–20 August, Cherry Hill, NJ.

APPENDIX: STRAIN–DISPLACEMENT MATRICES AND LAMINATE STIFFNESSES

$$[H] = \begin{bmatrix} \dfrac{\partial \psi_i}{\partial x} & 0 & 0 \\ 0 & \dfrac{\partial \psi_i}{\partial y} & 0 \\ \dfrac{\partial \psi_i}{\partial y} & \dfrac{\partial \psi_i}{\partial x} & 0 \\ 0 & 0 & \dfrac{\partial \psi_i}{\partial x} \\ 0 & 0 & \dfrac{\partial \psi_i}{\partial y} \end{bmatrix}$$

$$[H'] = \begin{bmatrix} \dfrac{\partial \psi_i}{\partial x} & 0 \\ 0 & \dfrac{\partial \psi_i}{\partial y} \\ \dfrac{\partial \psi_i}{\partial y} & \dfrac{\partial \psi_i}{\partial x} \\ \psi_i & 0 \\ 0 & \psi_i \end{bmatrix} \quad \text{for } i = 1, 2, \ldots, m.$$

$$A_{pq} = \sum_{k=1}^{n} \int_{z_k}^{z_{k+1}} Q_{pq}^{(k)} \, dz \quad (p, q = 1, 2, 6, 4, 5)$$

$$B_{pq}^{i} = \sum_{k=1}^{n} \int_{z_k}^{z_{k+1}} Q_{pq}^{(k)} \phi_i \, dz \quad (p, q = 1, 2, 6)$$

$$D_{pq}^{ij} = \sum_{k=1}^{n} \int_{z_k}^{z_{k+1}} Q_{pq}^{(k)} \phi_i \phi_j \, dz \quad (p, q = 1, 2, 6)$$

$$B_{pq}^{i} = \sum_{k=1}^{n} \int_{z_k}^{z_{k+1}} Q_{pq}^{(k)} \frac{d\phi_i}{dz} \, dz \quad (p, q = 4, 5)$$

$$D_{pq}^{ij} = \sum_{k=1}^{n} \int_{z_k}^{z_{k+1}} Q_{pq}^{(k)} \frac{d\phi_i}{dz} \frac{d\phi_j}{dz} dz \quad (p, q = 4, 5)$$